International Journal of Nanomedicine

Dovepress
open access to scientific and medical research

Open Access Full Text Article

ORIGINAL RESEARCH

Improving Longitudinal Transversal Relaxation Of Gadolinium Chelate Using Silica Coating Magnetite Nanoparticles

This article was published in the following Dove Press journal:
International Journal of Nanomedicine

Kai Xu[1,2]
Heng Liu[3]
Junfeng Zhang[1,2]
Haipeng Tong[1,2]
Zhenghuan Zhao[4]
Weiguo Zhang[1,2]

[1]Department of Radiology, Daping Hospital, Army Medical Center of PLA, Army Medical University, Chongqing 400042, People's Republic of China; [2]Chongqing Clinical Research Center for Imaging and Nuclear Medicine, Chongqing 400042, People's Republic of China; [3]Department of Radiology, PLA Rocket Force Characteristic Medical Center, Beijing 100088, People's Republic of China; [4]Department of Pharmaceutical Engineering, College of Pharmaceutical Sciences, Southwest University, Chongqing 400716, People's Republic of China

Introduction and objective: Precisely and sensitively diagnosing diseases especially early and accurate tumor diagnosis in clinical magnetic resonance (MR) scanner is a highly demanding but challenging task. Gadolinium (Gd) chelate is the most common T_1 magnetic resonance imaging (MRI) contrast agent at present. However, traditional Gd-chelates are suffering from low relaxivity, which hampers its application in clinical diagnosis. Currently, the development of nano-sized Gd based T_1 contrast agent, such as incorporating gadolinium chelate into nanocarriers, is an attractive and feasible strategy to enhance the T_1 contrast capacity of Gd chelate. The objective of this study is to improve the T_1 contrast ability of Gd-chelate by synthesizing nanoparticles (NPs) for accurate and early diagnosis in clinical diseases.

Methods: Reverse microemulsion method was used to coat iron oxide (IO) with tunable silica shell and form cores of NPs IO@SiO_2 at step one, then Gd-chelate was loaded on the surface of silica-coated iron oxide NPs. Finally, Gd-based silica coating magnetite NPs IO@SiO_2-DTPA-Gd was developed and tested the ability to detect tumor cells on the cellular and in vivo level.

Results: The r_1 value of IO@SiO_2-DTPA-Gd NPs with the silica shell thickness of 12 nm was about 33.6 $mM^{-1}s^{-1}$, which was approximately 6 times higher than Gd-DTPA, and based on its high T_1 contrast ability, IO@SiO_2-DTPA-Gd NPs could effectively detect tumor cells on the cellular and in vivo level.

Conclusion: Our findings revealed the improvement of T_1 relaxation was not only because of the increase of molecular tumbling time caused by the IO@SiO_2 nanocarrier but also the generated magnetic field caused by the IO core. This nanostructure with high T_1 contrast ability may open a new approach to construct high-performance T_1 contrast agent.

Keywords: gadolinium chelate, silica, iron oxide, nanoparticles, T_1 relaxivity, tumbling time

Correspondence: Zhenghuan Zhao
Department of Pharmaceutical Engineering, College of Pharmaceutical Sciences, Southwest University, No. 2 Tiansheng Road, Beibei District, Chongqing 400715, People's Republic of China
Tel +86 236 875 7621
Fax +86 236 875 7620
Email roddirck@swu.edu.cn

Weiguo Zhang
Department of Radiology, Daping Hospital, 10th Changjiang Road, Yuzhong District, Chongqing 400042, People's Republic of China
Tel +86 236 875 7621
Fax +86 236 875 7620
Email wgzhang01@163.com

Introduction

Magnetic resonance imaging has been widely used in clinical diagnosis due to its high spatial and temporal resolution, non-invasive and non-radioactive imaging.[1,2] However, its sensitivity and specificity are insufficient to provide enough signal in clinical MR scanner to achieve the diagnosis, especially early and accurate tumor diagnosis. Thus, various MRI contrast agents have been developed, such as gadolinium-based,[3,4] iron-based,[5–7] and manganese-based agents,[8–11] to improve its accuracy and sensitivity. Compared to iron or manganese element, gadolinium exhibits long electronic relaxation time and more unpaired electrons. These advantages endow Gd-chelates to be the most common T_1 MRI contrast agent to shorten longitudinal

submit your manuscript | www.dovepress.com
DovePress
http://doi.org/10.2147/IJN.S211974

relaxation time of protons and assist cancer diagnosis in clinical. Currently, different Gd-chelates have been approved by the Food and Drug Administration (FDA) for clinical imaging, such as Gd-DTPA (Magnevist) and Gd-DOTA (Dotarem). However, Gd-chelates are suffering from low relaxivity and contrast efficiency, which hamper the application on clinical diagnosis. Based on the classical Solomon-Bloembergen-Morgan (SBM) theory, the T_1 relaxivity is determined by a few parameters, including proton residence lifetime, molecular tumbling time and the number of coordinating.[12,13] In theory, along with the increase of molecular tumbling time, number of coordinating, and decrease of proton residence lifetime, the T_1 contrast capacity of contrast agent is improved. Nano-sized materials exhibit significantly slower molecular tumbling than small molecules, which could improve T_1 MRI contrast ability of Gd-based agent.[14–16] Thus, development of nano-sized Gd based T_1 contrast agent, such as incorporating Gd-chelates into nanocarriers, is an attractive and feasible strategy to enhance the T_1 contrast capacity of Gd-chelates.

On the basis of its high biocompatibility and T_2 contrast capacity, superparamagnetic iron oxide NPs have been used as the nanocarrier for constructing T_1/T_2 dual-modal MRI contrast agent to achieve tumor diagnosis.[17–19] However, the effect of iron oxide NPs which could affect the T_1 contrast ability of Gd-chelate was ignored. Previous research indicated that the magnetic field generated by superparamagnetic T_2 contrast agent might disturb the relaxation process of proton caused by the T_1 contrast agent, which may quench the acceleration effect of Gd-chelate to proton relaxation.[20–22] It should be noted that this quenching effect decreases with the increase of the distance between T_2 contrast agent and T_1 contrast agent. Meanwhile, the magnetic field induced by the T_2 contrast agent may result in T_1 spin alignment in the same direction, which lead to the enhancement of T_1 effect.[23–26] Thus, the distance between T_2 and T_1 contrast agent may determine the effect of T_2 contrast agent to a T_1 contrast agent. The Strategy of loading Gd-chelate on the surface of iron oxide NPs with suitable distance may develop a new T_1 contrast agent with high performance.

Recently, silica coating has been widely used to improve the biocompatibility and stability of biomedical materials.[27–29] Among all approaches, the reverse microemulsion method has been widely used to coat hydrophobic NPs with tunable silica shell.[30,31] Furthermore, the silica coating shell is easy to couple and label functional molecules based on the abundant functional group.[32,33] These unique features endow it to be the best tool to adjust the distance between iron oxide NPs and Gd-chelate and discuss the distance effect on T_1 contrast ability of Gd-chelate. Herein, we developed a strategy to improve the T_1 contrast ability of Gd-chelate by loading the Gd-chelate on the surface of silica-coated iron oxide NPs (IO@SiO_2-DTPA-Gd). The r_1 value of IO@SiO_2-DTPA-Gd NPs with the silica shell thickness of ~ 12 nm was about 33.6 $mM^{-1}s^{-1}$, which was approximately 6 times higher than Gd-DTPA. Further analysis indicated that the improvement of T_1 relaxation was not only because of the increase of molecular tumbling time caused by the IO@SiO_2 nanocarrier but also the generated magnetic field caused by the IO core. In addition, the improvement effect of T_1 relaxation increased with the growth of silica shell thickness. Based on its high T_1 contrast ability, IO@SiO_2-DTPA-Gd NPs can effectively detect tumor cells on the cellular and in vivo level. This nanostructure with high T_1 contrast ability may open a new approach to construct high-performance T_1 contrast agent.

Materials And Methods

Materials

Oleic acid (tech 90%), tetraethylorthosilicate (TEOS 99.9%), (3-aminopropyl) triethoxysilane (APTES 97%), 1-octadecene (90%), and oleic acid (90%) were purchased from Alfa Aesar. (Shanghai, China); p-SCN−Bn−DTPA was purchased from Macrocyclics; Sodium oleate, iron chlorides, hexane, isopropanol, ammonium hydroxide, and ethanol were purchased from Sinopharm Chemical Reagent Co. Ltd. (Shanghai, China). All chemicals were used as received without further purification.

Characterizations

Transmission electron microscopy (TEM) images were taken on JEOL JEM-2100 at 200 kV. The X-ray diffraction (XRD) patterns were obtained on the Rigaku Ultima IV system. The iron and gadolinium concentrations in NPs were measured with inductively coupled plasma atomic emission spectroscopy (ICP-AES). The absorbance was measured using a microplate reader (MultiSkan FC microplate reader, Thermo scientific). The MRI testing and T_1 relaxation time measurements were tested at a 0.5 T NMR120-Analyst NMR Analyzing&Imaging system (Niumag Corporation, Shanghai, China).

Preparation Of Iron Oxide NPs

In a typical experiment, 0.8 g iron-oleate (0.88 mmol) synthesized as aforementioned and 142 μL oleic acid (0.44 mmol)

were dissolved in 12 mL 1-octadecene at room temperature. The mixture was degassed in vacuum for 30 min and backfilled with argon to remove any low volatile impurities and oxygen at room temperature. After that, the reaction solution was heated to reflux with a constant heating rate of 3.3 °C min^{-1} and kept at that temperature for 1 h. The resultant solution was then cooled to room temperature and mixed with 30 mL isopropanol to precipitate the NPs. The NPs were separated by centrifugation and washed three times with ethanol. After washing, the NPs were dissolved in hexane for long term storage at 4 °C.

Preparation Of IO@SiO_2-NH_2 NPs

The reverse microemulsion method was used to prepare IO@SiO_2-NH_2 NPs. In a typical experiment, we added 1.2 mL of Co-520, 2 mL of iron oxide NPs solution (0.8 mg/mL), 200 μL of TEOS, and 400 μL of ammonia into 20 mL of cyclohexane. After 16 h reaction at room temperature, we added 20 μL of APTES to modify the amino group on the surface. The resultant solution was mixed with 40 mL of ethanol to precipitate the nanomaterials at 14,000 rpm. The nanomaterials were washed three times with ethanol. After washing, this nanomaterial was dissolved in ultrapure water (18.2 MΩ·cm) at room temperature for further use. By adjusting the amount of TEOS, the IO@SiO_2-NH_2 NPs with different shell thicknesses could be synthesized.

Conjugation Of DTPA-Gd On IO@SiO_2-NH_2 NPs

The conjugation of DTPA-Gd was achieved by reacting the IO@SiO_2-NH_2 NPs with p-SCN-DTPA with the molar ratio of 1:3. The NPs were separated by centrifugation and washed three times with water to remove the free p-SCN-DTPA. After washing, the NPs were dissolved in 10 mL $GdCl_3.6H_2O$ (194.7 mg) solution (pH 7.4) and stirred overnight. The resultant product was centrifuged and redispersed in water three times and dissolved in water for long term storage at 4 °C.

Measurement Of MR Relaxivities Of NPs

To measure the T_1 relaxivities, samples with different gadolinium ion concentrations were dispersed in 1% agarose solution. The T_1 relaxation times for all the samples were measured by a 0.5 T NMI20-Analyst NMR system and used to calculate the relaxation rates of the samples. The T_1-weighted MRI images for the samples were acquired using the MSE sequence as the following parameters: TR/TE = 100/12 ms, 256 × 256 matrices, thickness = 1mm, NS = 2.

Cell Culture

HeLa cells were purchased from the Cell Bank of Chinese Academy of Sciences (Shanghai, China). HeLa cells were cultured in Dulbecco's Modified Eagle's Medium (DMEM medium) supplemented with 10% fetal bovine serum (FBS, Hyclone) and antibiotics (100 mg/mL streptomycin and 100 U/mL penicillin) and maintained in a humidified atmosphere of 5% CO_2 at 37 °C.

Cytotoxicity Evaluation

Cells were seeded into a 96-well plate with a density of 5×10^3 cells/well in the culture medium and incubated in the atmosphere of 5% CO_2 at 37 °C for 12 h. The cells were then incubated with IO@SiO_2-DTPA-Gd NPs at a serial of Gd concentrations for 24 h. Each experiment in the same concentration was performed in five times. Subsequently, the culture medium was removed, we replaced the growth medium with DMEM containing 0.5 mg/mL of 3-(4, 5-dimethylthiazol-2-yl)-2, 5-diphenyltetrazolium bromide (MTT) and incubated for another 4 h at 37 °C. After discarding the culture medium, 100 μL of DMSO was added to dissolve the precipitates and the resulting solution was measured for absorbance at 492 nm using a MultiSkan FC microplate reader (Thermo scientific).

Cellular Imaging

HeLa cells were seeded with a density of 5×10^3 cells/well in the culture medium and incubated in the atmosphere of 5% CO_2 at 37 °C for 12 h. The cells were then incubated with IO@SiO_2-DTPA-GdNPs and DTPA-Gd for 6 h. Each experiment in the same concentration was performed in three wells. We then centrifuged the cells at 200 g for 5 min to harvest them. Then, we concentrated the cells at the button of the EP tube by centrifugation and performed T_1-weighted MRI imaging on a 0.5 T NMI20-Analyst NMR system. The samples were scanned using a multi-echo T_1-weighted fast spin-echo imaging sequence (TR/TE = 100/12 ms, 256 × 256 matrices, thickness = 1mm, NS = 16).

In Vivo MR Imaging

For establishment of HeLa tumor model, female Balb/c nude mice (25 ± 2 g, 4–5 weeks) were supplied by Center of Experimental Animals, Daping Hospital, China. All animal experiments were executed according to the protocol approved by the Animal Care and Use Committee of Army Medical University, China. Xenografted tumor models were made by subcutaneous inoculation of 10^6 HeLa cells suspended in 100 μL PBS at the right back of mice. When the

tumor reached 100 mm^3, the mice bearing tumor were intravenously injected IO@SiO_2-DTPA-Gd NPs (2 mg Gd/kg body weight). The T_1-weighted MRI imaging was performed on the 7 T Animal MRI (Bruker) and the MR images were acquired using the following parameters: TR/TE = 1500/8 ms, 256 × 256 matrices, thickness = 1mm, FOV = 250×250 mm. The MR images were sequentially acquired at pre-injection and 15, 30, 45, 60 and 120 min post-injection.

Statistical Analysis

Statistical analysis was performed using the Student's *t*-test for unpaired data, p values of less than 0.05 were accepted as a statistically significant difference compared to controls.

Results And Discussion

Synthesis And Characterization

To obtain silica-coated iron oxide nanostructure to improve the T_1 relaxation of Gd-chelate, Fe_3O_4 (IO) NPs were synthesized by thermal decomposition of iron-oleate in 1-octadecene. TEM images (Figure 1A) indicated that the as-prepared product was monodispersed spherical NPs in high yield. The diameters of these products were about 12 nm. Additionally, the high-resolution TEM (HRTEM)

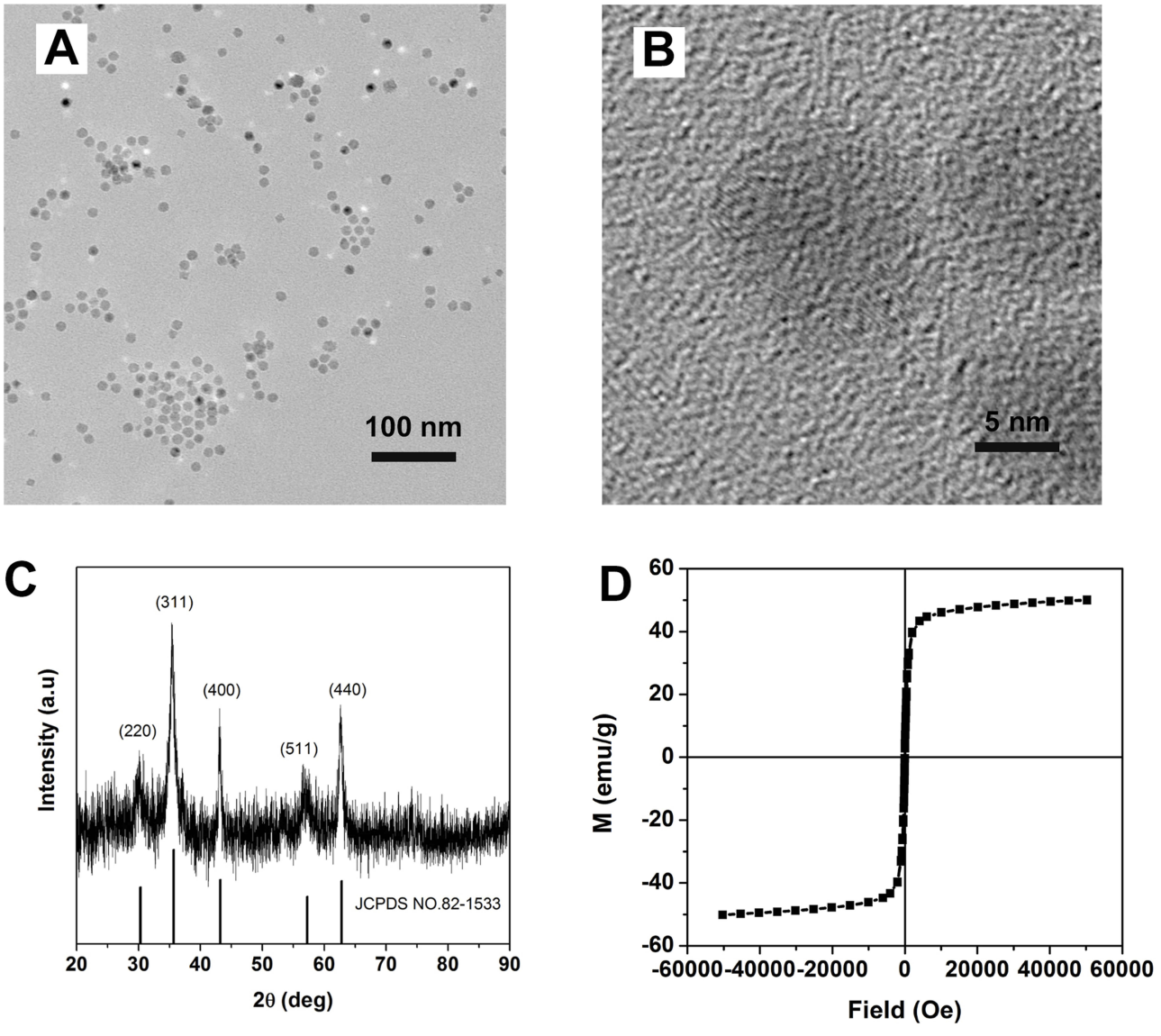

Figure 1 Characteristic of IO nanoparticles. (**A**) TEM and (**B**) HRTEM images of Fe_3O_4 nanoparticles. (**C**) XRD analysis of IO nanoparticles, indicating the typical magnetite diffractogram pattern. (**D**) M-H curve of IO.

Abbreviations: IO, iron oxide; TEM, transmission electron microscopy; HRTEM, high-resolution TEM; XRD, X-ray diffraction.

images (Figure 1B) showed the uniform lattice fringes across the whole NPs, revealing its good crystallinity and implying its good magnetic property. Further X-ray powder diffraction pattern analysis (Figure 1C) confirmed that the product exhibited the typical IO diffractogram pattern (JCPDS number 82–1533). We then analyzed the magnetic properties of as-prepared IO NPs by the superconducting quantum interference device magnetometer at 300 K. It appeared that the IO NPs showed a smooth *M-H* curve (Figure 1D) with no hysteresis at ambient temperature, suggesting the superparamagnetic behavior. Moreover, the M_s value of IO NPs was about 49 emu/g. These magnetic features endowed IO NPs to generate the magnetic field under the local filed to affect the T_1 relaxation of Gd-chelate.

We further coated the IO NPs by silica shell through a reverse microemulsion method with TEOS and (3-aminopropyl) APTES (Figure 2A). TEM images showed the typical spherical core/shell structure with the average shell thickness of ~12 nm (Figure 2B). Moreover, all product showed uniform coating of silica on IO NPs with single core and no core-free silica NPs existed. These features ensured it to be the suitable candidate for coupling Gd-chelate to construct new T_1 contrast agent with uniform ability. In addition, the morphology and size of single-core IO NPs maintained the same before and after coating (Figure 2B and C), enabling IO@SiO_2 with magnetic ability to affect the T_1 relaxation of Gd-chelate. The conjugation of Gd-chelate on the surface of IO@SiO_2 was achieved through the combination between amino groups on IO@SiO_2 and isothiocyanate of DTPA. ICP-AES analyses indicated that the Gd to Fe ratio is about 0.1:1. The TEM image showed that the IO@SiO_2-DTPA-Gd NPs exhibited similar size and morphology to that of IO@SiO_2 NPs (Figure 2C and D). Furthermore, the IO@SiO_2-DTPA-Gd NPs showed high colloidally stable in water at room temperature, which was essential for further biological application.

MR Relaxivities Investigation

To evaluate the MRI performance of IO@SiO_2-DTPA-Gd NPs, we detected its T_1 relaxivity by a 0.5 T MRI scanner. In

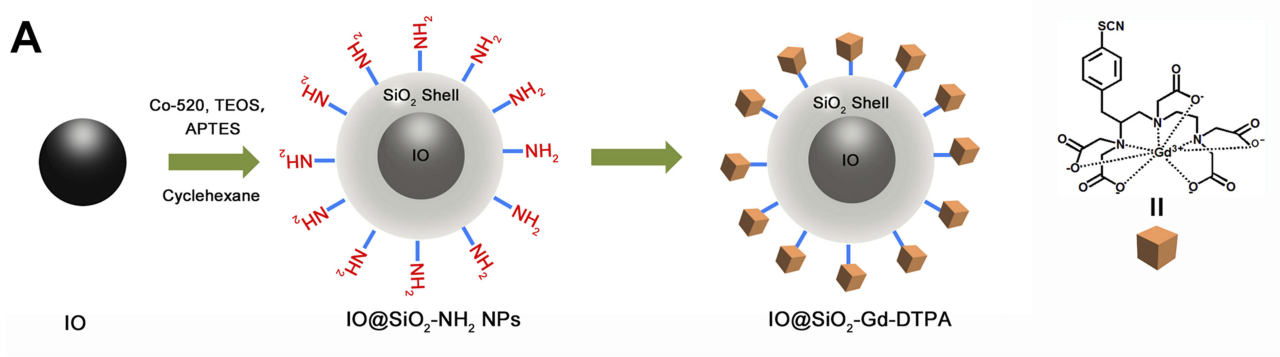

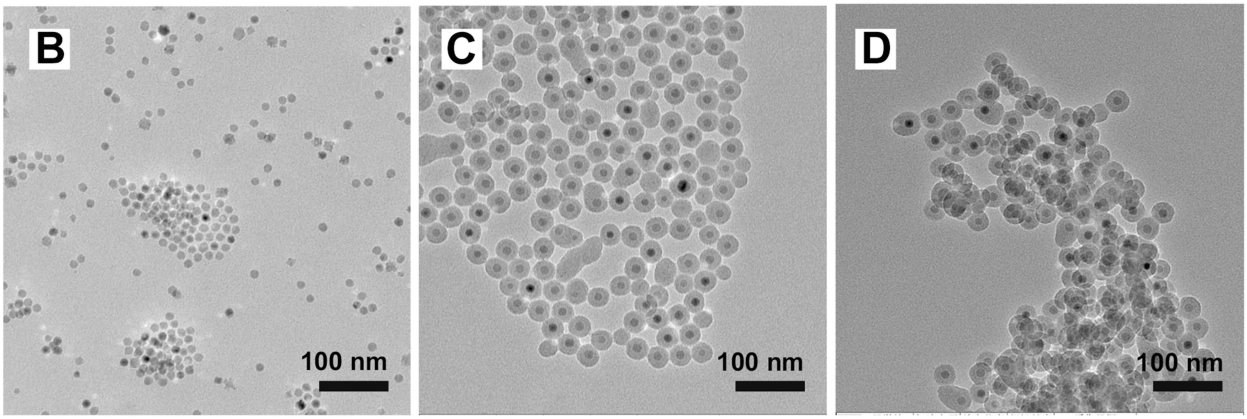

Figure 2 Synthesis of IO@SiO_2-DTPA-Gd NPs. (**A**) schematic cartoon illustrates the synthesis of IO@SiO_2-DTPA-Gd. TEM images of (**B**) IO core, (**C**) IO@SiO_2, and (**D**) IO@SiO_2-DTPA-Gd.
Abbreviations: Gd, gadolinium; IO, iron oxide; TEM, transmission electron microscopy; NPs, nanoparticles.

addition, DTPA-Gd was used for comparison (Figure 3A). T_1 relaxation analyses indicated that IO@SiO_2-DTPA-Gd NPs showed significantly higher T_1 contrast ability than free DTPA-Gd (Figure 3B and C). The r_1 value of IO@SiO_2-DTPA-Gd NPs was approximately 33.6 $mM^{-1}s^{-1}$ (Figure S1), which was about 6 times higher than that of DTPA-Gd (5.5 $mM^{-1}s^{-1}$). Consistent with the r_1 values analyses, IO@SiO_2-DTPA-Gd NPs exhibited better T_1 contrast imaging ability than free DTPA-Gd at the same concentration of Gd. Since the IO@SiO_2 showed negligible T_1 contrast ability (Figure S2), the improved T_1 contrast ability could be mainly ascribed to the improvement of molecular tumbling time of DTPA-Gd caused by the nanocarrier.[34,35] Additionally, the magnetic field induced by the T_2 contrast agent may also result in T_1 spin alignment in the same direction and enhancement of T_1 effect. To investigate whether the magnetic IO@SiO_2 core could improve the T_1 relaxation of DTPA-Gd, we synthesized SiO_2-DTPA-Gd with similar size as the control group (Figure 4A). TEM analyses showed that SiO_2-DTPA-Gd exhibited a similar size to IO@SiO_2-DTPA-Gd NPs (Figure 4B), implying the similar molecular tumbling time of SiO_2-DTPA-Gd and IO@SiO_2-DTPA-Gd NPs. These results could exclude the effect of molecular tumbling time on further T_1 relaxation analyses of SiO_2-DTPA-Gd and IO@SiO_2-DTPA-Gd NPs. We detected the T_1 relaxation of SiO_2-DTPA-Gd and IO@SiO_2-DTPA-Gd NPs by a 0.5 T MRI scanner (Figure 4C and D). Interestingly, it appeared that SiO_2-DTPA-Gd (22.1 $mM^{-1}s^{-1}$) showed notable higher T_1 relaxation than DTPA-Gd (5.5 $mM^{-1}s^{-1}$), which could be attributed to the increase of molecular tumbling time (Figure S3). It's worth note that the r_1 value of IO@SiO_2-DTPA-Gd NPs was 33.6 $mM^{-1}s^{-1}$, which was significantly higher than that of SiO_2-DTPA-Gd. Considering that IO@SiO_2-DTPA-Gd and SiO_2-DTPA-Gd NPs had the similar molecular tumbling time, these results clearly indicated

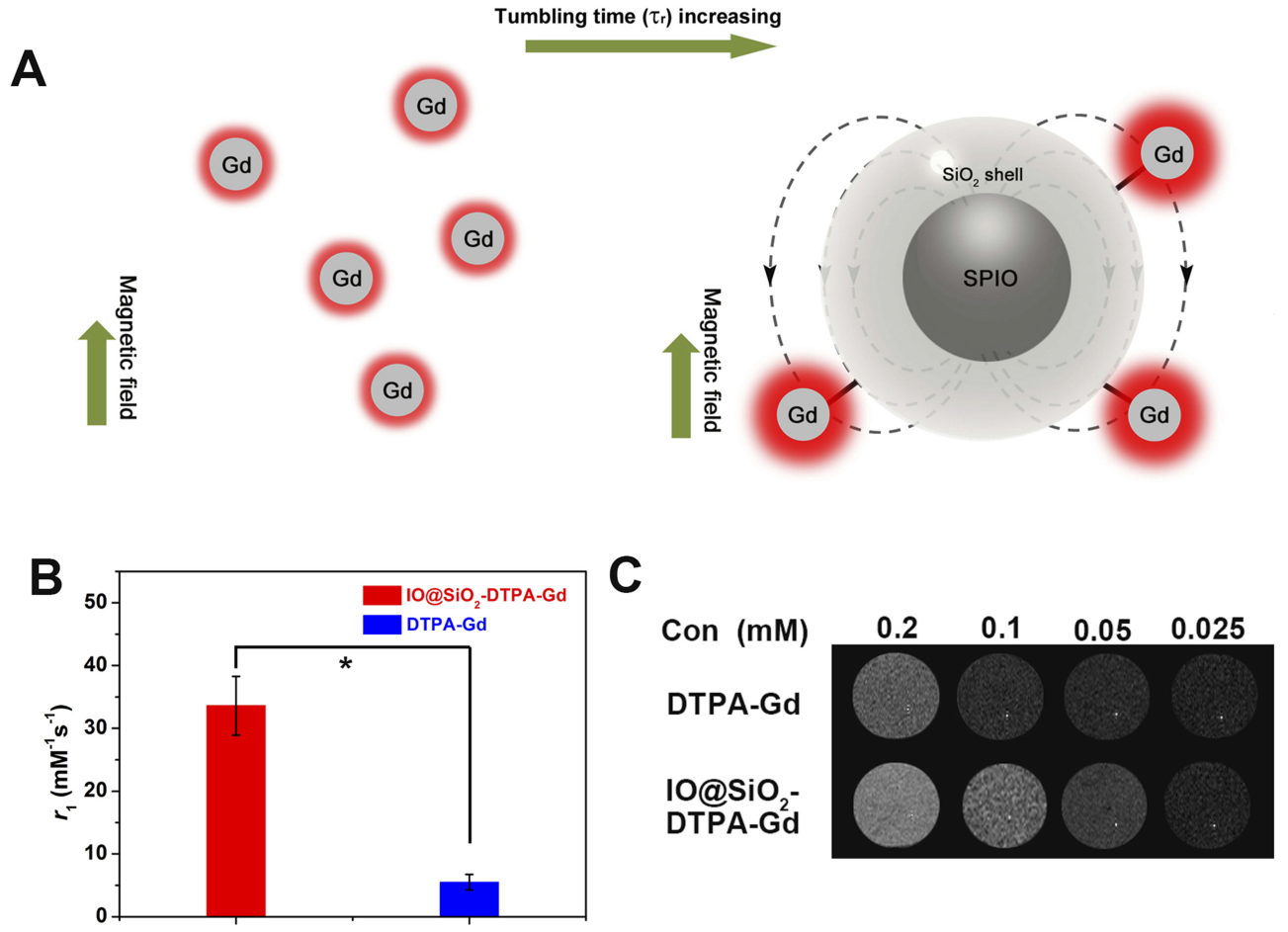

Figure 3 T_1 relaxation analysis of IO@SiO_2-DTPA-Gd NPs. (**A**) Schematic cartoons illustrate the increased molecular tumbling time result in the improve of IO@SiO_2-DTPA-Gd T_1 relaxation compared to DTPA-Gd. (**B**) T_1 relaxation analyses of IO@SiO_2-DTPA-Gd and DTPA-Gd, $p < 0.05$ (*). (**C**) T_1-weighted images of DTPA-Gd and IO@SiO_2-DTPA-Gd at different concentration.
Abbreviations: Gd, gadolinium; IO, iron oxide; NPs, nanoparticles.

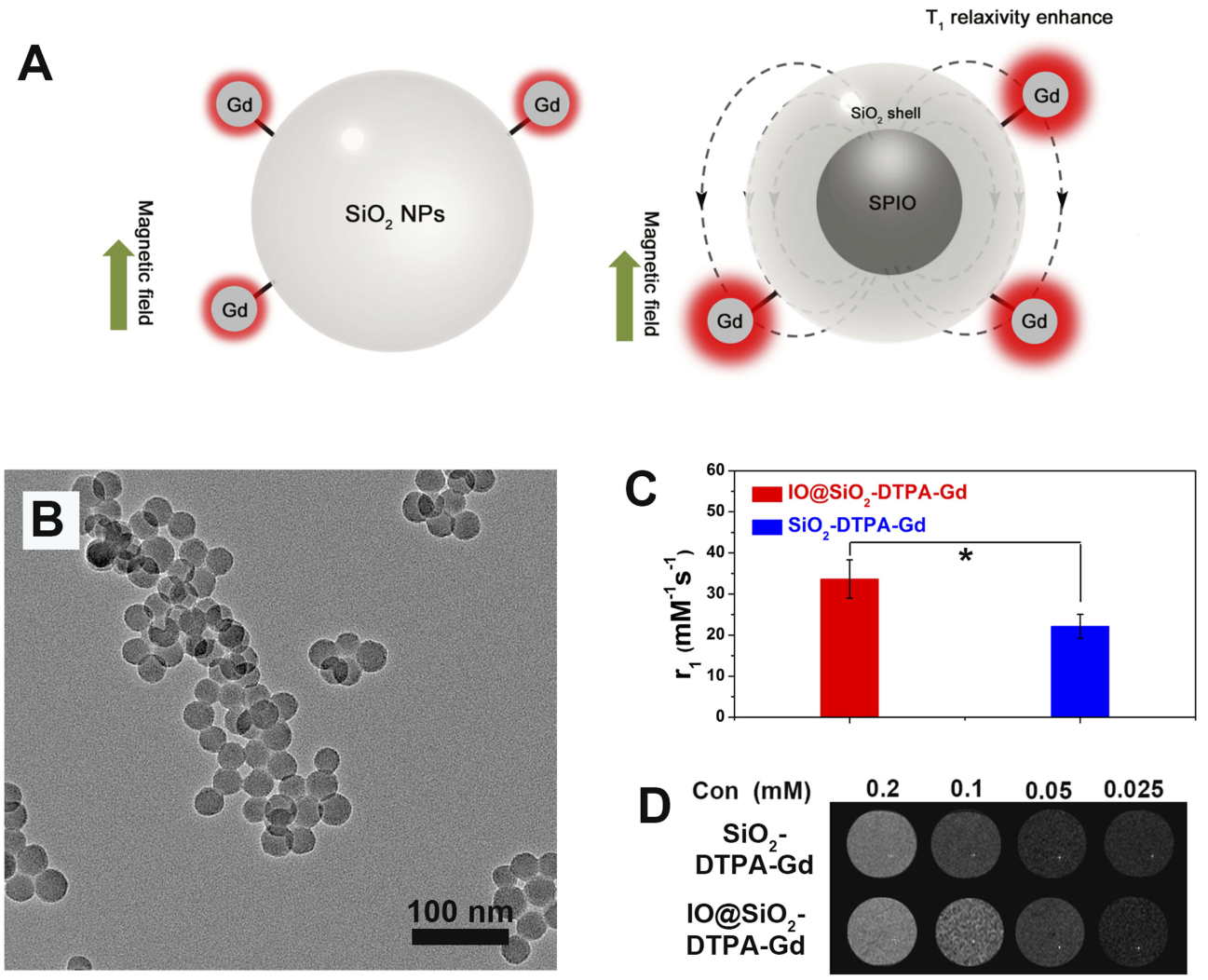

Figure 4 Effect of the IO core to the T_1 relaxation of IO@SiO_2-DTPA-Gd NPs. (**A**) schematic cartoons illustrate the IO core is another reason to improve IO@SiO_2-DTPA-Gd NPs T_1 relaxation. (**B**) TEM images of SiO_2-DTPA-Gd with the similar size to IO@SiO_2-DTPA-Gd NPs. (**C**) T_1 relaxation analyses of IO@SiO_2-DTPA-Gd and SiO_2-DTPA-Gd NPs, $p < 0.05$ (*). (**D**) T_1-weighted images of SiO_2-DTPA-Gd and IO@SiO_2-DTPA-Gd NPs at different concentration.
Abbreviations: Gd, gadolinium; IO, iron oxide; TEM, transmission electron microscopy, NPs, nanoparticles.

that the improved T_1 relaxation of IO@SiO_2-DTPA-Gd NPs was not only caused by the increased molecular tumbling time but also caused by the magnetite core of IO@SiO_2. Since the increments caused by the increase of molecular tumbling time was larger than that of introducing of magnetite, molecular tumbling time increase was the main reason to elevate the r_1 value of IO@SiO_2-DTPA-Gd NPs. Further T_1-weighted photon images revealed that the T_1 signal increases of IO@SiO_2-DTPA-Gd NPs were more obvious than that of SiO_2-DTPA-Gd, which endowed it with the ability to be a potential candidate for disease diagnosis.

We further assessed the effect of the SiO_2 thickness on the T_1 contrast ability of IO@SiO_2-DTPA-Gd NPs (Figure 5A). We synthesized IO@SiO_2-DTPA-Gd NPs with the silica thickness of 0, 5, and 12 nm by reverse microemulsion method through tuning the amount of TEOS. TEM images indicated that the thickness of the silica shell increased with the increase of TEOS ratio (Figure 5B and D). More importantly, all products showed the single core structure without core-free silica nanosphere. This feature endowed these products as suitable samples to discuss the effect of silica shell thickness to T_1 relaxation of IO@SiO_2-DTPA-Gd NPs. T_1 relaxation analyses indicated that the r_1 values of IO@SiO_2-DTPA-Gd NPs with a thickness of 0, 5, and 12 nm were 9.6, 14.8, and 33.6 $mM^{-1}s^{-1}$, respectively (Figure 5E and F). These results revealed that the T_1 contrast ability of IO@SiO_2-DTPA-Gd increased with the increase of shell thickness. It should be noted that IO@SiO_2-DTPA-Gd with the silica thickness of 0 and 5 nm even showed remarkable

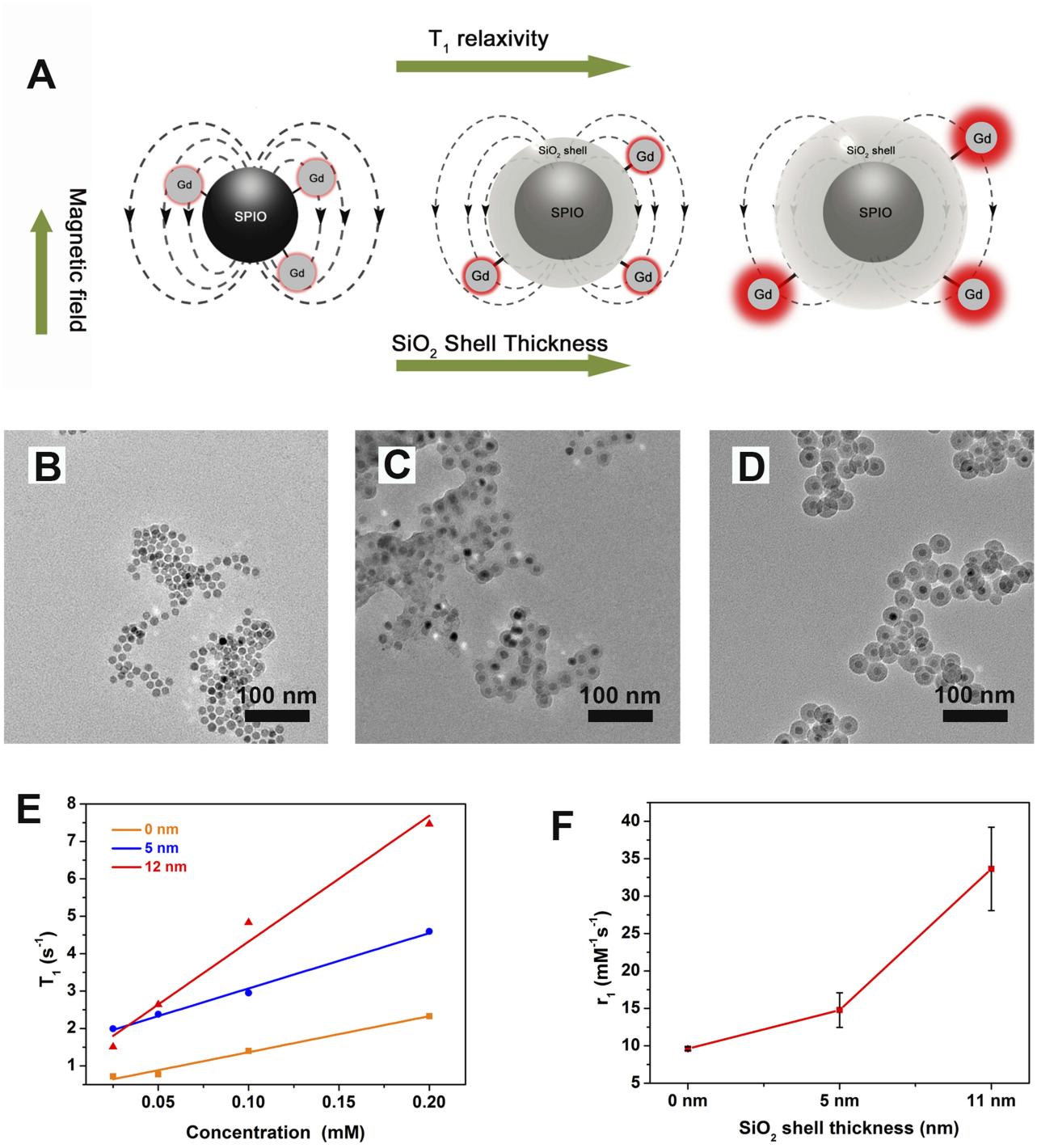

Figure 5 Effect of the silica shell thickness to the T_1 relaxation of IO@SiO_2-DTPA-Gd NPs. (**A**) schematic cartoons illustrate the Effect of the silica shell thickness to the T_1 relaxation of IO@SiO_2-DTPA-Gd NPs. TEM images of (**B**) IO-DTPA-Gd, (**C**) IO@SiO_2-DTPA-Gd NPs with the thickness of 5 nm, and (**D**) IO@SiO_2-DTPA-Gd NPs with the thickness of 12 nm. (**E**) T_1 relaxation of IO-DTPA-Gd, IO@SiO_2-DTPA-Gd NPs with the thickness of 5 nm, and IO@SiO_2-DTPA-Gd NPs with the thickness of 12 nm. (**F**) r_1 values change curve of IO-DTPA-Gd, IO@SiO_2-DTPA-Gd NPs with the thickness of 5 nm, and IO@SiO_2-DTPA-Gd NPs with the thickness of 12 nm.
Abbreviations: Gd, gadolinium; IO, iron oxide; TEM, transmission electron microscopy, NPs, nanoparticles.

lower r_1 value than SiO_2-DTPA-Gd. These results could be ascribed to the quenching effect of T_2 contrast agent to the DTPA-Gd and indicated that the effect of magnetite core to surface DTPA-Gd was decided by the distance.[20,36] The distance between magnetite and DTPA-Gd was more close, the quenching effect of magnetite to DTPA-Gd was strong enough to hinder the T_1 relaxation of DTPA-Gd. Along with the increase of distance between magnetite and DTPA-Gd,

quench effect decreased and showed the enhancement effect of magnetite to DTPA-Gd.

Celluar Imaging And Cytotoxicity Evaluation

To evaluate the T_1 contrast ability of IO@SiO_2-DTPA-Gd NPs on the cellular level, we incubated IO@SiO_2-DTPA-Gd NPs with HeLa cells and conducted T_1-weighted imaging. It appeared that the cells incubated with IO@SiO_2-DTPA-Gd NPs showed a remarkable bright signal in T_1-weighted imaging, which was significantly higher than that of DTPA-Gd treated group (Figure 6A). The signal-to-noise ratio analyses (Figure 6B) further confirmed that IO@SiO_2-DTPA-Gd NPs group was much higher than the DTPA-Gd group, demonstrating IO@SiO_2-DTPA-Gd could be used as a contrast agent to achieve T_1 contrast imaging. The cytotoxicity of IO@SiO_2-DTPA-Gd NPs was detected via the MTT assay to assess its biocompatibility. It appeared that no obvious decrease in cell viability which could be observed after incubation of IO@SiO_2-DTPA-Gd NPs with Hela cells for 24 h (Figure S4). Neither apparent agglomeration nor precipitation was observed for IO@SiO_2-DTPA-Gd NPs after incubation for 24 h in water and different physiological media including PBS buffer, DMEM culture medium, and blood serum (Figure S5). These results indicated that IO@SiO_2-DTPA-Gd NPs showed the good stability and high biocompatibility, which ensured it as a contrast agent for further biological application.

In Vivo MR Imaging

Considering the good biocompatibility and high contrast capability of IO@SiO_2-DTPA-Gd NPs, in vivo MR imaging was then performed for tumor detection. The T_1-weighted MR images exhibited that T_1 signal of tumor region gradually increased and showed sufficient signal to detect tumor in mice (Figure 7A). To quantify the contrast enhancement, the SNR ratio was calculated according to the T_1-weighted MR images. It appeared that the post-injection signal was much higher than the pre-injection signal (about 1.3 fold at 30 min), demonstrating IO@SiO_2-DTPA-Gd could also be used as a contrast agent to achieve in vivo T_1 contrast imaging (Figure 7B). But due to the lack of modification and tumor targeting module, less accumulation of NPs existed in tumor and resident time was short. Hence, the modification such as PEGylation and tumor targeting module or the tumor microenvironment response module should be added in the further experiment to enhance the retention effect and the visibility of tumor in vivo.

Conclusion

In conclusion, we developed a high-performance nano-sized T_1 contrast agent IO@SiO_2-DTPA-Gd NPs by loading the Gd-chelate on the surface of silica-coated iron oxide NPs. The synthesized NPs IO@SiO_2-DTPA-Gd showed high r_1 value, which was approximately 6 times higher than Gd-DTPA when the silica shell thickness of ~ 12 nm. In addition, to reveal the underlying mechanism, IO@SiO_2, SiO_2-DTPA-Gd, and IO@SiO_2-DTPA-Gd were synthesized respectively and compared to each other. These results clearly indicated that the improved T_1 relaxation of IO@SiO_2-DTPA-Gd NPs was not only caused by the increased molecular tumbling time but also caused by the magnetite core of IO@SiO_2. Additionally, the increase of distance between magnetite core and DTPA-Gd could also reduce the quenching effect and

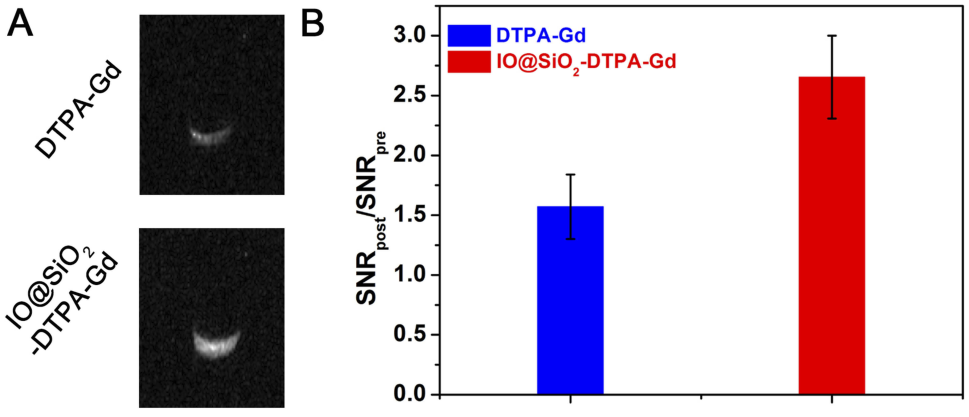

Figure 6 Cellular level imaging. (**A**) T_1-weighted MR images of cells incubated with DTPA-Gd and IO@SiO_2-DTPA-Gd NPs. (**B**) Signal-to-noise ratio changes of T_1-weighted images of Hela cells incubated with DTPA-Gd and IO@SiO_2-DTPA-Gd NPs.
Abbreviations: Gd, gadolinium; IO, iron oxide, NPs, nanoparticles.

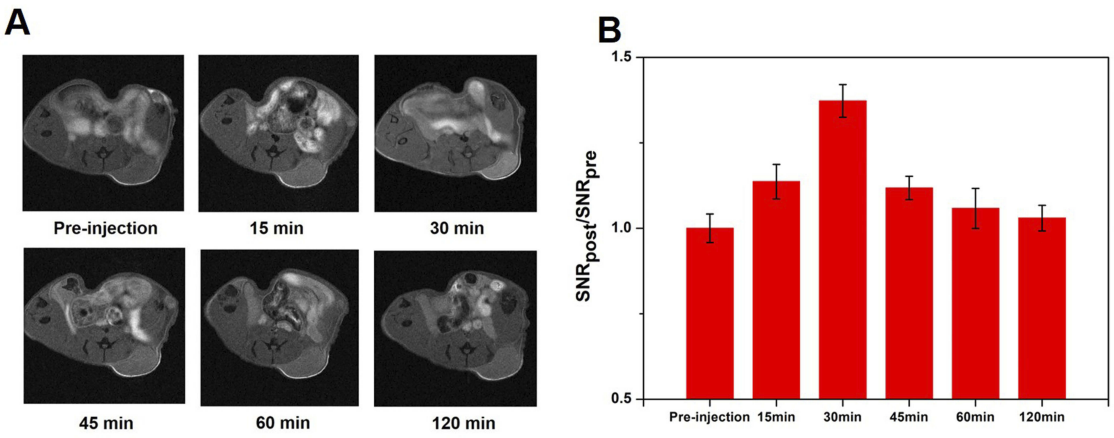

Figure 7 In vivo MR imaging. (**A**) T_1-weighted MR images of tumor at pre-injection and 15, 30, 45, 60 and 120 min after intravenous injection of IO@SiO_2-DTPA-Gd NPs, respectively (**B**) Signal-to-noise ratio changes of T_1-weighted images of tumor at different time after administration of IO@SiO_2-DTPA-Gd NPs.
Abbreviations: Gd, gadolinium; IO, iron oxide, NPs, nanoparticles.

show the enhancement effect of magnetite core to DTPA-Gd. Moreover, the remarkable bright signal in T_1-weighted imaging of IO@SiO_2-DTPA-Gd NPs incubating cells and in vivo MR imaging indicated that IO@SiO_2-DTPA-Gd NPs could be the potential MRI contrast agent for the future clinical application.

Acknowledgments

This work was supported by the National Natural Science Foundation of China (NSFC) (Grant Nos. 81571660 and 81601607) and the National Natural Science Foundation of China (NSFC) (Grant No. 81871421).

Disclosure

The authors report no conflicts of interest in this work.

References

1. Shin T-H, Choi Y, Kim S, Cheon J. Recent advances in magnetic nanoparticle-based multi-modal imaging. *Chem Soc Rev*. 2015;44(14):4501–4516. doi:10.1039/c4cs00345d
2. Fan W, Yung B, Huang P, Chen X. Nanotechnology for multimodal synergistic cancer therapy. *Chem Rev*. 2017;117(22):13566–13638. doi:10.1021/acs.chemrev.7b00258
3. Johnson NJJ, He S, Nguyen Huu VA, Almutairi A. Compact micellization: a strategy for Ultrahigh T1 magnetic resonance contrast with gadolinium-based nanocrystals. *ACS Nano*. 2016;10(9):8299–8307. doi:10.1021/acsnano.6b02559
4. Qin L, Sun Z-Y, Cheng K, et al. Zwitterionic manganese and gadolinium metal–organic frameworks as efficient contrast agents for in vivo magnetic resonance imaging. *ACS Appl Mater Interfaces*. 2017;9(47):41378–41386. doi:10.1021/acsami.7b09608
5. Peng Y-K, Lui CNP, Chen Y-W, et al. Engineering of single magnetic particle carrier for living brain cell imaging: a tunable T1-/T2-/dual-modal contrast agent for magnetic resonance imaging application. *Chem Mater*. 2017;29(10):4411–4417. doi:10.1021/acs.chemmater.7b00884
6. Zhao Z, Chi X, Yang L, et al. Cation exchange of anisotropic-shaped magnetite nanoparticles generates high-relaxivity contrast agents for liver tumor imaging. *Chem Mater*. 2016;28(10):3497–3506. doi:10.1021/acs.chemmater.6b01256
7. Zhao Z, Zhou Z, Bao J, et al. Octapod iron oxide nanoparticles as high-performance T_2 contrast agents for magnetic resonance imaging. *Nat Commun*. 2013;4:2266. doi:10.1038/ncomms3266
8. Na HB, Lee JH, An K, et al. Development of a T1 contrast agent for magnetic resonance imaging using MnO nanoparticles. *Angew Chem-Int Ed*. 2007;119(28):5493–5497. doi:10.1002/ange.200604775
9. Zhao Z, Wang X, Zhang Z, et al. Real-time monitoring of arsenic trioxide release and delivery by activatable T1 imaging. *ACS Nano*. 2015;9(3):2749–2759. doi:10.1021/nn506640h
10. Zhao Z, Bao J, Fu C, Lei M, Cheng J. Controllable synthesis of manganese oxide nanostructures from 0-D to 3-D and mechanistic investigation of internal relation between structure and T1 relaxivity. *Chem Mater*. 2017;29(24):10455–10468. doi:10.1021/acs.chemmater.7b04100
11. Lei M, Fu C, Cheng X, et al. Activated surface charge-reversal manganese oxide nanocubes with high surface-to-volume ratio for accurate magnetic resonance tumor imaging. *Adv Funct Mater*. 2017;27(30):1700978. doi:10.1002/adfm.201700978
12. Werner EJ, Datta A, Jocher CJ, Raymond KN. High-relaxivity MRI contrast agents: where coordination chemistry meets medical imaging. *Angew Chem-Int Ed*. 2008;47(45):8568–8580. doi:10.1002/anie.200800212
13. Ni K, Zhao Z, Zhang Z, et al. Geometrically confined ultrasmall gadolinium oxide nanoparticles boost the T1 contrast ability. *Nanoscale*. 2016;8(6):3768–3774. doi:10.1039/c5nr08402d
14. Ananta JS, Godin B, Sethi R, et al. Geometrical confinement of gadolinium-based contrast agents in nanoporous particles enhances T1 contrast. *Nat Nanotechnol*. 2010;5:815. doi:10.1038/nnano.2010.203
15. Paik T, Tr G, Am P, Yun H, Cb M. Designing tripodal and triangular gadolinium oxide nanoplates and self-assembled nanofibrils as potential multimodal bioimaging probes. *ACS Nano*. 2013;7(3):2850–2859. doi:10.1021/nn4004583
16. Li F, Li Z, Jin X, et al. Ultra-small gadolinium oxide nanocrystal sensitization of non-small-cell lung cancer cells toward X-ray irradiation by promoting cytostatic autophagy. *Int J Nanomedicine*. 2019;14:2415–2431. doi:10.2147/IJN.S193676
17. Bae KH, Kim YB, Lee Y, Hwang J, Park H, Park TG. Bioinspired synthesis and characterization of gadolinium-labeled magnetite nanoparticles for dual contrast T1- and T2-weighted magnetic resonance imaging. *Bioconjugate Chem*. 2010;21(3):505–512. doi:10.1021/bc900424u

18. Yang H, Zhuang Y, Sun Y, et al. Targeted dual-contrast T1- and T2-weighted magnetic resonance imaging of tumors using multifunctional gadolinium-labeled superparamagnetic iron oxide nanoparticles. *Biomaterials*. 2011;32(20):4584–4593. doi:10.1016/j.biomaterials.2011.03.018
19. Li F, Zhi D, Luo Y, et al. Core/shell Fe3O4/Gd2O3 nanocubes as T1–T2 dual modal MRI contrast agents. *Nanoscale*. 2016;8(25):12826–12833. doi:10.1039/c6nr02620f
20. J-s C, Lee J-H, Shin T-H, Song H-T, Kim EY, Cheon J. Self-confirming "AND" logic nanoparticles for fault-free MRI. *J Am Chem Soc*. 2010;132(32):11015–11017. doi:10.1021/ja104503g
21. Zhu X, Lin H, Wang L, et al. Activatable T1 relaxivity recovery nanoconjugates for kinetic and sensitive analysis of matrix metalloprotease 2. *ACS Appl Mater Interfaces*. 2017;9(26):21688–21696. doi:10.1021/acsami.7b05389
22. J-s C, Kim S, Yoo D, et al. Distance-dependent magnetic resonance tuning as a versatile MRI sensing platform for biological targets. *Nat Mater*. 2017;16:537. doi:10.1038/nmat4846
23. Gallo J, Harriss BI, Hernández-Gil J, Bañobre-López M, Long NJ. Probing T1–T2 interactions and their imaging implications through a thermally responsive nanoprobe. *Nanoscale*. 2017;9(31):11318–11326. doi:10.1039/c7nr01733b
24. Keasberry NA, Bañobre-López M, Wood C, Stasiuk GJ, Gallo J, Long NJ. Tuning the relaxation rates of dual-mode T1/T2 nanoparticle contrast agents: a study into the ideal system. *Nanoscale*. 2015;7(38):16119–16128. doi:10.1039/c5nr04400f
25. Zhou Z, Huang D, Bao J, et al. A synergistically enhanced T1–T2 dual-modal contrast agent. *Adv Mater*. 2012;24(46):6223–6228. doi:10.1002/adma.201203169
26. Santra S, Jativa SD, Kaittanis C, Normand G, Grimm J, Perez JM. Gadolinium-encapsulating iron oxide nanoprobe as activatable NMR/MRI contrast agent. *ACS Nano*. 2012;6(8):7281–7294. doi:10.1021/nn302393e
27. He Q, Shi J. MSN anti-cancer nanomedicines: chemotherapy enhancement, overcoming of drug resistance, and metastasis inhibition. *Adv Mater*. 2014;26(3):391–411. doi:10.1002/adma.201303123
28. Chen Y, Chen H, Zeng D, et al. Core/shell structured hollow mesoporous nanocapsules: a potential platform for simultaneous cell imaging and anticancer drug delivery. *ACS Nano*. 2010;4(10):6001–6013. doi:10.1021/nn1015117
29. Cao YC. Synthesis of square gadolinium-oxide nanoplates. *J Am Chem Soc*. 2004;126(24):7456–7457. doi:10.1021/ja0481676
30. Hl D, Yx Z, Wang S, Jm X, Sc X, Gh L. Fe3O4@SiO2 Core/shell nanoparticles: the silica coating regulations with a single core for different core sizes and shell thicknesses. *Chem Mater*. 2012;24(23):4572–4580. doi:10.1021/cm302828d
31. Yi DK, Lee SS, Papaefthymiou GC, Ying JY. Nanoparticle architectures templated by SiO2/Fe2O3 nanocomposites. *Chem Mater*. 2006;18(3):614–619. doi:10.1021/cm0512979
32. Sato T, Shimosato T, Klinman DM. Silicosis and lung cancer: current perspectives. *Lung Cancer*. 2018;9:91–101. doi:10.2147/LCTT.S156376
33. Das M, Yi DK, An SS. Analyses of protein corona on bare and silica-coated gold nanorods against four mammalian cells. *Int J Nanomedicine*. 2015;10:1521–1545. doi:10.2147/IJN.S76187
34. Wang L, Lin H, Ma L, et al. Albumin-based nanoparticles loaded with hydrophobic gadolinium chelates as T1–T2 dual-mode contrast agents for accurate liver tumor imaging. *Nanoscale*. 2017;9(13):4516–4523. doi:10.1039/c7nr01134b
35. Wang L, Zhu X, Tang X, et al. A multiple gadolinium complex decorated fullerene as A highly sensitive T1 contrast agent. *Chem Commun*. 2015;51(21):4390–4393. doi:10.1039/C5CC00285K
36. Shin T-H, J-s C, Yun S, et al. T1 and T2 dual-mode MRI contrast agent for enhancing accuracy by engineered nanomaterials. *ACS Nano*. 2014;8(4):3393–3401. doi:10.1021/nn405977t